

# FUSE Observations of RX J0513.9–6951

J.B. Hutchings<sup>1</sup>, A.P. Cowley<sup>2</sup>, R. Mann<sup>1</sup>, P.C. Schmidtke<sup>2</sup>, & D. Crampton<sup>1</sup>

<sup>1</sup>Herzberg Institute of Astrophysics, NRC of Canada, Victoria, B.C. V8X 4M6, Canada;  
john.hutchings@nrc.ca

<sup>2</sup>Department of Physics & Astronomy, Arizona State University, Tempe, AZ, 85287-1504;  
anne.cowley@asu.edu, paul.schmidtke@asu.edu

## ABSTRACT

FUSE observations were obtained in July 2003 during 1.2 cycles of the 0.76-day binary orbit of RX J0513.9–6951. Radial velocity measurements of the broad O VI emission profile show a semiamplitude of  $K \sim 26 \text{ km s}^{-1}$ , which is much smaller than the value of  $117 \text{ km s}^{-1}$  measured from 2001 FUSE data. Narrow O VI emissions show no measurable velocity variation. The mean velocity of the broad O VI emission is red-shifted by  $\sim 500 \text{ km s}^{-1}$  with respect to both the systemic and narrow emission-line velocities. Spectral difference plots show phase-related changes in the broad emission profile. Other phase-related changes such as line and continuum variations are also smaller than in the 2001 spectra. We describe a moving broad absorption feature near  $1020 \text{ \AA}$  as possible O VI outflow associated with a precessing jet. We discuss the implications for the stellar masses if the 2003 broad O VI velocities outline the compact star's orbital motion.

*Subject headings:* X-rays: binaries, stars: white dwarfs

## 1. Introduction

Supersoft X-ray sources are close binary systems thought to contain a rapidly accreting white dwarf and a low-mass donor star. Direct mass determinations for these systems have been difficult to make since the low-mass star is much fainter than the bright accretion disk. It seemed possible that in the Large Magellanic Cloud system RX J0513–695 the far ultraviolet O VI emission lines might outline the accreting star's orbital motion, hence revealing information about the stellar masses.

RX J0513–6951 is the most luminous of the known supersoft X-ray binary systems in the Milky Way or the Magellanic Clouds. The 0.76-day binary period is well determined from optical light curves observed over many years by the MACHO project (e.g. Alcock et al. 1996; Cowley et al. 2002). The small variation in the orbital light curve ( $\Delta m \sim 0.06 \text{ mag}$ ) and the low-amplitude of the velocity curve from optical emission lines (semiamplitude  $K \sim 11 \text{ km s}^{-1}$ ) suggest the system is viewed nearly pole-on. Optical and X-ray fluxes show antiphased long-term high/low states (Reinsch et al. 1996), and optical spectra show the velocity curve changes between the high and low states (Cowley et al. 2002). Additionally, the system shows evidence of bi-polar jets in some optical emission lines, with velocities of  $\pm \sim 4000 \text{ km s}^{-1}$  (Crampton et al. 1996; Southwell et al. 1996). There is also evidence of a long-term photometric period of  $\sim 83.2 \text{ days}$  (Cowley et al. 2002) which might be related to precession of the accretion disk.

Using FUSE data obtained in 2001, Hutchings et al. (2002) found the O VI resonance doublet was composed of a broad, blended emission feature, with narrow O VI emission superimposed. The broad blend

showed a moderately high velocity semi-amplitude ( $K \sim 117 \text{ km s}^{-1}$ ), which implied rather large stellar masses if due to orbital motion of the compact star (Hutchings et al. 2002). To determine if this motion was a transient event or a permanent feature of the system, we obtained additional FUSE spectra in July of 2003.

## 2. 2003 Data and Measurements

RX J0513.9–6951 was observed continuously (with earth occultations) on 2003 July 5 for 1.2 binary orbits. We use phases based on optical minimum light from Cowley et al. (2002):

$$T(\text{min}) = \text{JD } 2,448,858.099 \pm 0.001 + 0.7629434 \pm 0.0000020 \text{E days} \quad (= \text{MJD } 48857.599)$$

However, we note that although the photometry provides an accurate clock, the system’s low inclination suggests  $\Phi=0$  may not occur exactly at the superior conjunction of the compact star. Hence, although we know the relative phasing of variable features, the orientation of the stars with respect to the observer is somewhat uncertain.

The FUSE observations were processed as 15 individual spectra through the binary orbit phases, corresponding to the visibility windows during the observation period. Table 1 lists both the total observing time and that obtained during spacecraft nighttime. Count rates in all channels were steady, indicating that the telescope alignments were good. The long exposure windows show that we were close to the continuous viewing zone (CVZ). The airglow contamination was not correlated with the fraction of orbital night in each spectrum, so we did not separate the night and day portions of the observations. We note that the strength of the airglow emission in both epochs is similar. The mean FUSE spectrum from 915Å to 1100Å is shown in Fig. 1. To aid in understanding the spectrum, the upper dotted line in each panel shows the  $\text{H}_2$  absorption spectrum and the lower dashed line shows the position of the principal airglow lines.

### 2.1. The Line Spectrum

The O VI doublet (1032, 1038Å) remains the principal emission feature in the far ultraviolet spectrum. O VI continues to show both a broad (some 20Å wide), blended emission and sharp individual peaks (see Fig. 1 & 2). He II (1084Å) emission is also present, although it is badly blended with airglow lines, making its measurement very difficult. In Fig. 1 one can see that He II has a P-Cygni structure, with absorption on the violet side of the emission, although contaminated by both  $\text{H}_2$  absorption and airglow emission. We looked for, but did not find clear evidence for other possible emission lines such as N III (991Å) and C III (977, 1175Å). These wavelengths are too close to strong airglow lines which have been edited out of the spectrum shown in Fig. 1. Thus, emission from either N III or C III may contribute to the airglow feature which was removed. However, we do see narrow absorptions which are likely to be C III and N III, similar to the He II absorption, and suggest these lines may have a P Cyg profile. We note that optical spectra show weak, narrow emissions of O VI, N V, and C IV, but lower ionization lines (N III and C III) are probably not present.

In both the 2001 and 2003 FUSE spectra, absorption lines are found in the higher Lyman lines (as marked in Fig. 1 of Hutchings et al. 2002). Similar features at the Balmer lines are seen in optical spectra (e.g. Crampton et al. 1996).

In Fig. 1 & 2 we have plotted the H<sub>2</sub> absorption spectrum to show the reader that a number of the absorptions in the spectrum are due to local molecular hydrogen. In addition, the interstellar absorption of the C II doublet at 1036-7Å is clearly present, with radial velocity  $\sim +30$  km s<sup>-1</sup>, as compared to the systemic velocity of +280 km s<sup>-1</sup> (Crampton et al. 1996).

There is a strong dip in the spectra near 1020Å at both epochs. It appears to shift to a more positive wavelength in the 2003 spectra. It might possibly be associated with the narrow O VI line at 1032Å. If so, it could be a signature of outflowing gas with velocity near  $-3300$  km s<sup>-1</sup> and full width about 700 km s<sup>-1</sup>. A corresponding absorption associated with the 1038Å O VI line would be totally obscured by Lβ absorption and by strong airglow emission.

### 2.1.1. O VI Emission Lines

Figure 2 compares the 2001 and 2003 spectra in the region around the broad O VI emission feature. We show the mean spectra from each epoch, with the continuum flux difference removed by an offset of 1.3e-14 (raising the possibility of zero-point errors, which we discuss below). This figure shows that both the broad and narrow O VI emissions were stronger during the 2003 observations.

The sharp O VI emission peaks show a mean velocity of +320 km s<sup>-1</sup>, with a P-Cygni type absorption at  $\sim +30$  km s<sup>-1</sup>. These lines show a total radial velocity range of only  $\sim 15$  km s<sup>-1</sup> and no clear phase dependence. This small variation is comparable with measures of the interstellar absorptions of C II and H<sub>2</sub>. Thus, the scatter may represent the errors due to the wavelength calibrations and overall S/N. Note that optical spectra of He II show a semiamplitude of only  $K=11$  km s<sup>-1</sup>, which is within our scatter of our FUSE measurements. The He II 1084Å line is too badly blended with airglow emission to measure its velocity.

Figure 3 shows the broad O VI mean profile, with the absorptions and narrow emissions edited out (by removing the sharp airglow emissions and sharp interstellar absorptions to leave a smooth broad residual). The figure also shows the reflected outer wings, centered on the wavelength that gives the most compact symmetrical profile. To measure the velocity of this broad emission we used the mean edited spectrum as a template. This template was cross-correlated against the unedited individual spectra, and the centroid of the broad cross-correlation peak was recorded. This process was repeated for different versions of the edited template, and also using variously edited individual spectra. The centroids of the broad cross-correlation peaks were not very sensitive to these detailed variations of process, suggesting that we are indeed measuring a property of the broad emission. We also measured the same velocity shifts by fitting curves through the whole broad feature. This too, yielded similar values, but with considerably more scatter.

The resulting broad-emission O VI velocity curve from the cross-correlation process, described above, is shown in Figure 4. We note that we have small binary phase overlap in our data, and in all the quantities the overlap measures are in good agreement, supporting the assumption that we are measuring phase-related changes. Of course, we would prefer to have a second full cycle of observations to confirm this. These cross-correlation velocity values were used to fit a sine-curve, whose semiamplitude was found to be  $K\sim 26$  km s<sup>-1</sup>, much lower than the value of  $K\sim 117$  km s<sup>-1</sup> found in the 2001 data using the same measuring techniques. However, the full velocity range is more than twice as large of that of the optical He II lines. The phase of O VI maximum velocity occurs at  $\Phi_{phot}=0.77$ , compared to  $\Phi_{phot}=0.70$  in 2001. This phase difference is formally significant at the  $3\sigma$  level. While this amplitude is less than 1% of the full width of the feature, it is derived from a number of independent spectra, and the values appear to be

robust to details of the measuring procedure. We note also that the fit is based on measures that cover only 1.2 binary orbits, so that we may be seeing changes that are not binary-phase dependent. Against that, we also note that the values in the overlap phases do agree well.

The mean wavelength of the broad O VI line corresponds to a velocity of about  $+500 \text{ km s}^{-1}$  more positive than the mean of the narrow lines or the known systemic velocity of  $+280 \text{ km s}^{-1}$  (Crampton et al. 1996). Possible implications of this are discussed below.

The O VI broad emission flux was measured by integrating over the entire feature. The fluxes from the SiC channels were systematically lower than the LiF channels, by about 10%, but the phase-variation was similar in all channels. A plot of the mean of the LiF channels and the best-fit sine curve through them is shown in Fig. 4. The fit is significantly different from no variation at the  $3\sigma$  level. The variation range is about 6%, again much smaller than the  $\sim 30\%$  seen in 2001, and the phasing (if the variation is real) differs by  $\sim 0.2\text{P}$ .

Figure 5 shows difference plots between the individual spectra and the mean in the O VI region. The differences are heavily smoothed and amplified several times to reveal the broad changes in the profile, which appear principally as a dip that moves back and forth. The diagram also shows a dotted line indicating how the broad difference dip moves in orbital phase with a large velocity amplitude. This was quantified in the following way. The dip centroid was measured in each of the difference plots (roughly in the wavelength range  $1025$  to  $1050\text{\AA}$ ), and these values were used to derive a best-fit sine curve. The centroids are marked with dots in Figure 5. The fit to these with orbital phase has a semi-amplitude of  $3.8 \pm 0.9\text{\AA}$  (or  $K \sim 1100 \text{ km s}^{-1}$ ), with a zero point value of  $1036.9 \pm 0.6\text{\AA}$ , which is close to the mean wavelength of the O VI emission blend. This too is an indication that we are measuring changes in the broad emission feature, and not artifacts of the narrower blended features. Table 2 summarizes the fitted quantities.

### 2.1.2. *He II Emission at $1084\text{\AA}$*

In the 2001 data, He II ( $1084\text{\AA}$ ) was present, although it was blended with airglow features (the strongest being within  $0.1\text{\AA}$  of the systemic velocity of the binary), making it difficult to estimate its strength and any variations. The 2003 data have much longer observation windows which are close to being in the CVZ. We find that airglow is present at all times, and cannot be reduced by isolating the night-time data. He II appears to be weaker than in the 2001 spectra, but the width of the emission ( $\sim 4\text{\AA}$ ) and its central wavelength make it clear that there is He II emission blended with the airglow line. The He II line also shows P-Cygni type absorption on its violet edge (as do the narrow O VI emissions). Unfortunately the combination of airglow and  $\text{H}_2$  near  $1084\text{\AA}$  make measurement of He II impossible in the new FUSE spectra.

In optical spectra He II ( $4686\text{\AA}$ ) is always prominent, with wide wings (comparable with O VI) and a profile which varies over timescales much longer than the orbital period (see Crampton et al. 1996; Southwell et al. 1996). In addition, optical spectra also show narrow emission from the He II Pickering series lines.

### 2.1.3. *Hydrogen Absorption Lines*

The higher Lyman series lines show deep narrow absorptions, as in the 2001 data. Figure 6 shows some of the lines and the mean, plotted in radial velocity units. The absorptions are saturated and have

a flat saturated minimum to very high series numbers, so that we cannot tell if they have more than one component. The stronger Lyman lines have sharp (airglow) emission close to rest velocity, but the figure is made from lines that show no sign of these. We measured individual line wavelengths and also cross-correlated the region from 920-945Å with the mean spectrum. These measures indicate a very small phase-related radial velocity variation ( $K \sim 8 \text{ km s}^{-1}$ ), as summarized in Table 2 and shown in Figure 4. This variation is shifted by  $\sim 0.4$  in phase from the broad O VI emission velocity curve. It too has much lower amplitude than that found in the 2001 data, where the semiamplitude was found to be  $K \sim 54 \text{ km s}^{-1}$  and the velocity curve was antiphased with the broad O VI emission.

## 2.2. The Continuum

The 2003 continuum flux is lower by  $\sim 30\%$  (within the measuring uncertainty of  $\sim 10\%$ ) than 2001. It also shows smaller variations around the binary orbit. However, the flux changes from 2001 across the entire FUSE range are similar (to within 10%), so there appears to be no significant change in the spectral energy distribution with flux level. We have no ground-based or FUSE FES photometry to see if the lower flux in 2003 corresponded to a fainter optical magnitude.

Both the continuum flux level and the overall broad emission flux were measured as a function of orbital phase. The 2003 spectra show small ( $< 10\%$ ) changes in the continuum with phase (see Figure 3), but we do not observe the 60% flux rise between photometric phases 0.05 and 0.40 which was seen in the 2001 data. However, the FUSE light maximum still occurs near photometric phase  $\sim 0.2$ , as in 2001.

## 2.3. Long Period Variations

Cowley et al. (2002) found a long photometric period (83.2 day) in the MACHO data. The folded light curve shows an amplitude of  $\sim 0.05$ - $0.06$  magnitudes at optical wavelengths. This amplitude is consistent with the variation being due to inclination changes of a nearly face-on disk precessing over a small angle. For this simple assumption, the precession angle would be  $\sim 10^\circ$  or less for small orbital inclinations ( $i$  less than  $30^\circ$ ).

The same scenario would predict changes in the observed jet velocities, assuming they precesses normal to the accretion disk. Crampton et al. (1996) have measured jet velocities for three epochs, corresponding to 83-day phases of 0.99, 0.34, and 0.35. The precession scenario fixes the maximum velocity at maximum light. Fitting the Crampton et al. data to this model gives a semiamplitude of the jet velocity of  $K \sim 160 \text{ km s}^{-1}$ , with a mean value near  $4000 \text{ km s}^{-1}$ . This also gives possible values of the orbital inclination and precession angle which are similar to those implied by the low orbital light curve and optical velocity amplitude.

Thus, the long-period light curve and the jet velocity changes are compatible with a precession scenario in which  $i$  is less than  $30^\circ$  and the precession angle is less than  $10^\circ$ . These values also turn out to be consistent with the mass considerations shown in Fig. 7. Of course, many more complex scenarios are possible, since the observational evidence is minimal so far. Further observations would be very useful.

The FUSE observations have (by chance) similar long-period phasing to the Crampton et al. jet measurements. The 2001 data were taken at phase 0.99 and the 2003 data at phase 0.30. Although we see no evidence for narrow jet emission lines in the FUSE data as are found in optical data at He II 4686Å and

$H\beta$ , the width of the broad O VI blend is comparable to the jet velocities. We also note that the  $1020\text{\AA}$  absorption could be outflowing O VI gas, with a velocity of  $-3100\text{ km s}^{-1}$  ( $-3400\text{ km s}^{-1}$  in 2001). These velocities are lower than the measured jet velocities at the same phases, but the change is very similar. This would also be consistent with the precession scenario if the absorption arises in an outflow that has a wider opening angle than the jet itself.

### 3. Discussion and Conclusions

We find the O VI profile was stronger in 2003 in the innermost  $\pm 1800\text{ km s}^{-1}$ , but otherwise it still shows a very broad blended profile with both lines of the doublet having approximately equal strength. Thus, the lines presumably arise in an optically thick environment. The 2003 broad O VI velocity curve has a small semiamplitude of  $K \sim 26\text{ km s}^{-1}$  (much lower than the  $117\text{ km s}^{-1}$  seen in 2001), indicating that the earlier (and perhaps both) variations are not dominated by orbital motions. It is interesting that the derived binary phasing of the broad velocity variations is close to the same as the 2001 values. The maximum velocity occurs near quadrature (assuming minimum light is when the unheated side of the donor star is most visible). This is as expected if the velocities are related to the white dwarf's orbital motion, arising in its accretion disk. The change in amplitude, but little in phase, may indicate radial rather than azimuthal changes in the O VI disk structure.

The spectral difference plots show that there are phase-related profile changes arising over the whole broad profile. These can be represented as a wide absorption feature with velocity semiamplitude of  $K \sim 1100\text{ km s}^{-1}$ . This is far too high to be orbital motion, but it may arise in an asymmetry in the hot inner accretion disk around the compact star or be related to the inner parts of the high velocity jet which presumably lies near the line of sight. In this connection we note the broad absorption dip at  $\sim 1020\text{\AA}$  might also arise from O VI moving near the terminal velocity of the jet.

Although the O VI velocity phasing is close to the 2001 value, the line and continuum flux changes have different phasing. The narrow O VI emission peaks show no significant velocity changes. The Lyman absorptions, continuum flux, and O VI emission flux all have lower amplitudes than in the 2001 data. In addition, they all show different phasing, while they were nearly in phase in the 2001 data. The Lyman absorptions are saturated. They have a mean velocity of  $+200\text{ km s}^{-1}$ . No Lyman absorption lies at the sharp O VI velocity of  $+350\text{ km s}^{-1}$ , even if there are two components. The Lyman lines are variably contaminated by airglow and  $H_2$  absorption, so phase-related profile changes cannot be detected easily. The small phase-related velocity change could possibly be due to outflow from the system, as well as intervening absorbers not related to the binary system. The phasing of these velocity variations is consistent with origin in the gas stream from the donor star.

From the 2001 data we postulated that the broad O VI emission might arise in an orbit close to the white dwarf, and thus may represent its orbital velocity. Clearly, the substantial change between observing epochs indicates that the large velocity amplitude measured in 2001 must have arisen in mass flows within the system, not just from the white dwarf's orbital motion. However, for interest, in Figure 7 we show the implied masses for a star with the velocity semiamplitude of  $K = 26\text{ km s}^{-1}$  (from the 2003 O VI broad emission). The diagram also shows the boundaries set by assuming the jet velocities of  $\pm 4000\text{ km s}^{-1}$  are at the escape velocity of the white dwarf, and the broad line width ( $\sim 2500\text{ km s}^{-1}$ ) represents the rotational velocity of disk gas near the white dwarf's surface. These constraints define an area in the mass plot of Figure 7 bounded by the dashed lines. If we further assume that the mass losing star has evolved off the

main sequence, the allowed mass values are  $\sim 0.6\text{--}1.2M_{\odot}$  for the white dwarf and  $\sim 0.3\text{--}0.4M_{\odot}$  for the donor star.

Determining the mean velocity of the broad emission involves a number of assumptions. If it is symmetrical, as shown in Fig. 2, we find it is redshifted from the sharp emission components by  $\sim +500$  km  $\text{s}^{-1}$ , suggesting a possible gravitational redshift of gas near the surface of the white dwarf. The gravitational redshift of a  $0.65M_{\odot}$  WD is about  $300$  km  $\text{s}^{-1}$  and that of a  $1.4M_{\odot}$  WD is  $600$  km  $\text{s}^{-1}$ . Thus, the observed shift might be evidence that the WD is massive and that the O VI arises very close to its surface. The fact that the broad doublet lines are apparently of equal flux, indicates that they are formed in a high density region.

We thank Alex Fullerton for help with the FUSE data, and the referee for helpful comments.

Table 1.

Dataset D006010....	JD (mid-exp) 2452800 +	Exposure time, in sec		Photometric Phase <sup>a</sup>
		Total	Nighttime	
1001	25.81250	4075	915	0.535
1002	25.85938	4010	980	0.560
1003	25.91016	3885	1780	0.663
1004	25.96094	3936	1574	0.729
1005	26.00781	4221	354	0.791
1006	26.05859	4256	1950	0.857
1007	26.11719	5033	2110	0.934
2001	26.19922	4234	1700	0.041
2002	26.27344	4190	1450	0.139
2003	26.34375	4076	1110	0.231
2004	26.41797	4002	790	0.328
2005	26.49219	4088	530	0.425
2006	26.56250	4280	400	0.518
2007	26.63672	4439	491	0.615
2008	26.70703	4095	704	0.707

<sup>a</sup>Phases with respect to light minimum, which is not necessarily conjunction of the two stars. Ephemeris:  $T(\text{min}) = \text{JD } 2,448,858.099 \pm 0.001 + 0.7629434 \pm 0.0000020E$  (= MJD 48857.599), where  $T(\text{min})$  is minimum  $V$  light (Cowley et al. 2002).

Table 2.

Feature	Photometric Phase <sup>a</sup>	Semi-amplitude ( $\text{km s}^{-1}$ or %)	ME ( $\text{km s}^{-1}$ or %)
O VI broad emis	0.77±0.02	26±4 $\text{km s}^{-1}$	16 $\text{km s}^{-1}$
O VI broad diffs	0.76±0.04	1100±180 $\text{km s}^{-1}$	300 $\text{km s}^{-1}$
Ly narrow abs	0.40±0.04	8±2 $\text{km s}^{-1}$	8 $\text{km s}^{-1}$
1070Å continuum flux	0.16±0.10	1.5±1.0%	2%
O VI flux	0.93±0.05	2.8±0.8%	2.0%

<sup>a</sup>Phases with respect to  $V$  light minimum. Ephemeris:  $T(\text{min}) = \text{JD } 2,448,858.099 \pm 0.001 + 0.7629434 \pm 0.0000020E$  (from Cowley et al. 2002).



## REFERENCES

- Alcock, C., et al. 1996, MNRAS, 280, L49
- Cowley, A.P., Schmidtke, P.C., Crampton, D., & Hutchings, J.B. 1998, ApJ, 504, 854
- Cowley, A.P., Schmidtke, P.C., Crampton, D., & Hutchings, J.B. 2002, AJ, 124, 2233
- Crampton, D., Hutchings, J.B., Cowley, A.P., Schmidtke, P.C., McGrath, T.K., O’Donoghue, D., & Harrop-Allin, M.K. 1996, ApJ, 456, 320
- Hutchings, J.B., Winter, K., Cowley, A.P., Schmidtke, P.C., & Crampton, D. 2002, AJ, 124, 2833
- Reinsch, K., van Teeseling, A., Beuermann, K., & Abbott, T.M.C. 1996, A&A, 309, L11
- Southwell, K.A., Livio, M., Charles, P.A., O’Donoghue, D., & Sutherland, W.J. 1996, ApJ, 470, 1065

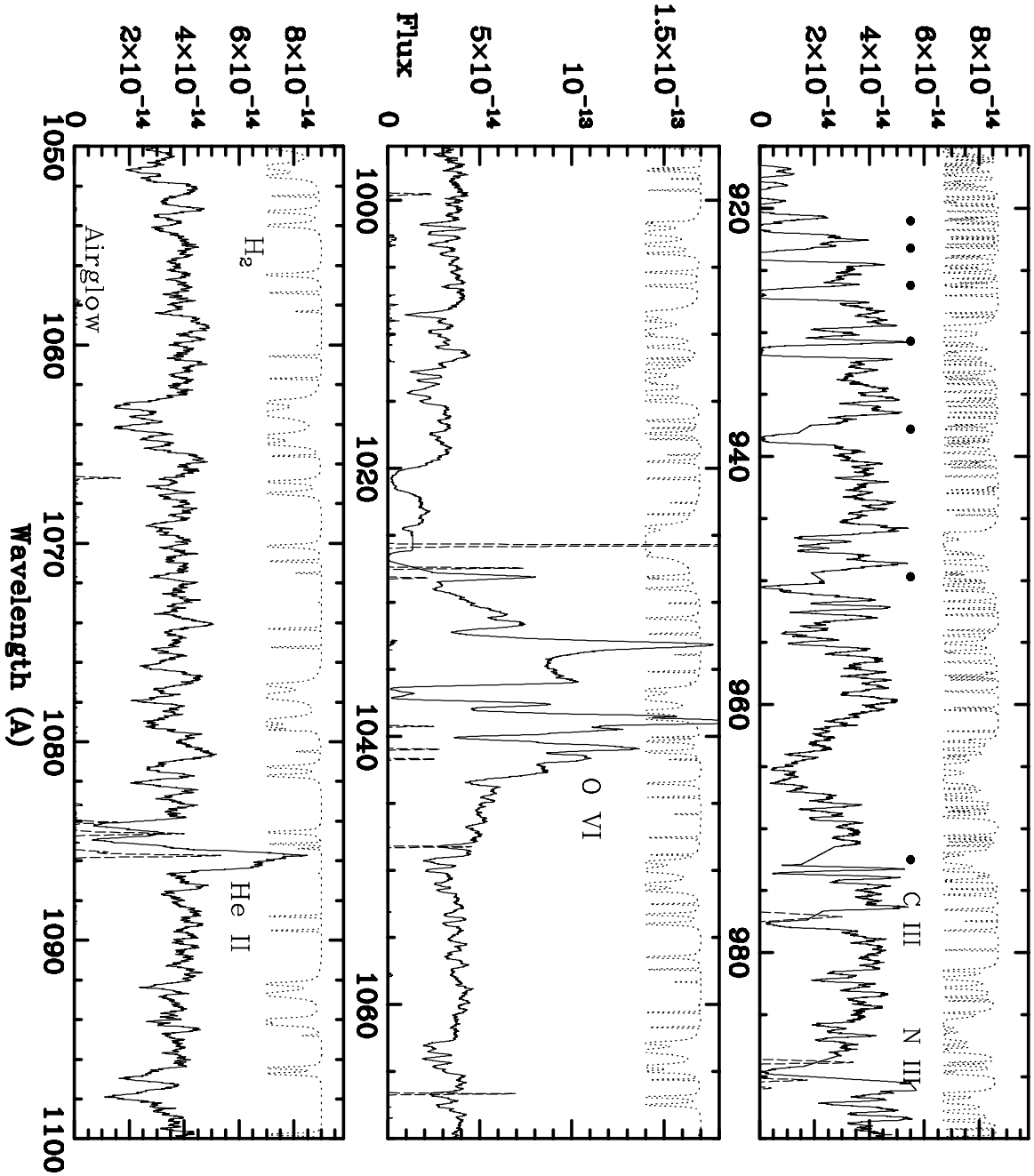


Fig. 1.— The mean FUSE spectrum of RX J0513.9–6951 (solid line). The dotted line at the top of each panel shows the positions and relative strengths of H<sub>2</sub> absorbers, and the lower dashed line shows the principal airglow features. Fluxes are in  $\text{erg cm}^{-2} \text{s}^{-1} \text{Å}^{-1}$ . The dots in the upper panel show the rest wavelengths of Lyman lines.

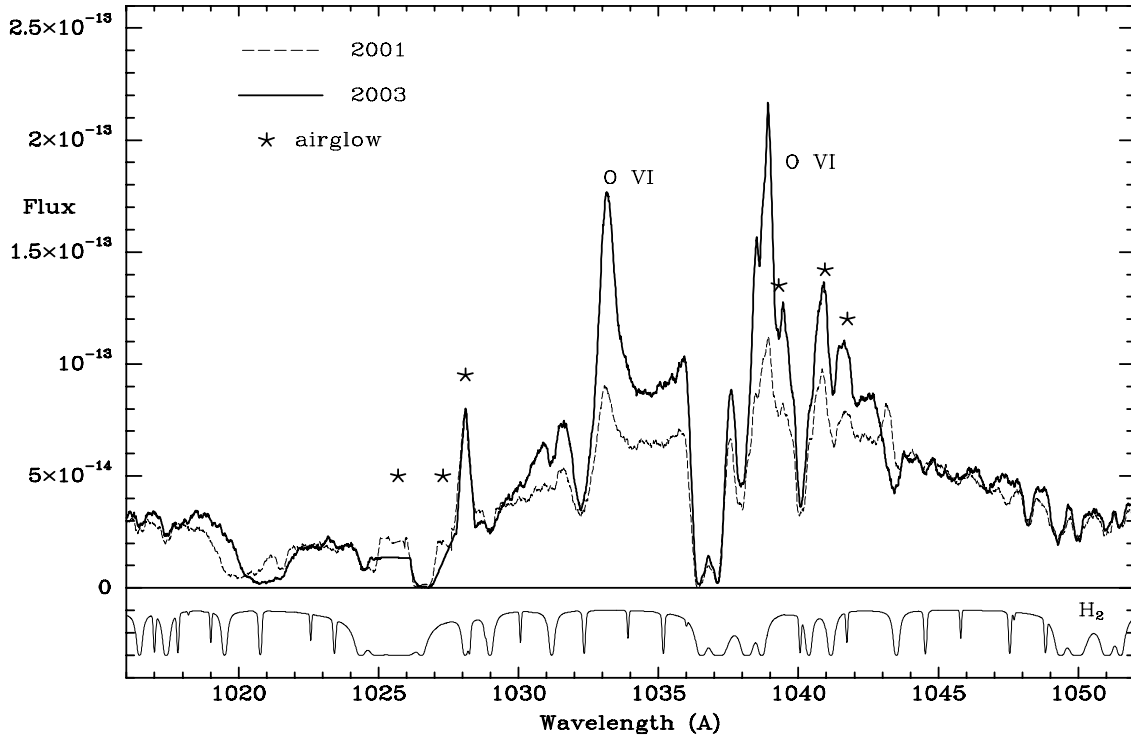


Fig. 2.— Mean spectra in O VI doublet region for the 2001 (dashed line) and 2003 (solid line) epochs. Fluxes are in  $\text{erg cm}^{-2} \text{s}^{-1} \text{\AA}^{-1}$ . The zero point has been adjusted for the 2001 spectrum by subtracting  $1.3 \times 10^{-15}$ , in order to match the continuum levels. The overall 2003 profile is higher in the central region, while the airglow and absorption features match well. H<sub>2</sub> absorbers can be identified from the model spectrum plotted in the lower panel. The strongest airglow lines (including Ly $\beta$  at 1026Å) have been edited out manually, but their positions are marked. Note the change in the position of the absorption feature near 1020-1Å.

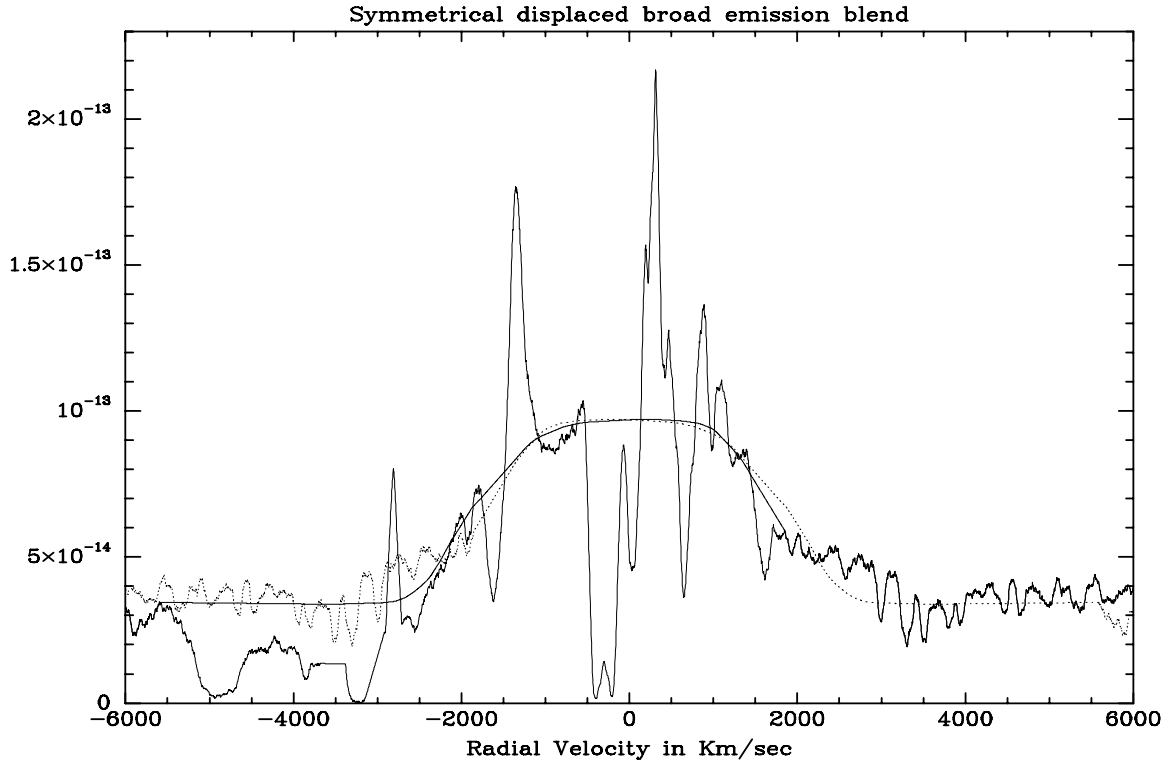


Fig. 3.— Mean broad O VI emission from the 2003 data, with the reflected profile (shown as a dotted line) superimposed. Fluxes are in  $\text{erg cm}^{-2} \text{s}^{-1} \text{\AA}^{-1}$ . To create this profile, we have edited out the sharp emissions and absorptions. The center of the broad line is arbitrarily set to zero velocity. The reflection wavelength is chosen to maximize the broad feature symmetry. Note that the center of the broad profile is positively displaced with respect to the average position of the narrow O VI emission by  $\sim 500 \text{ km s}^{-1}$ , as discussed in the text.

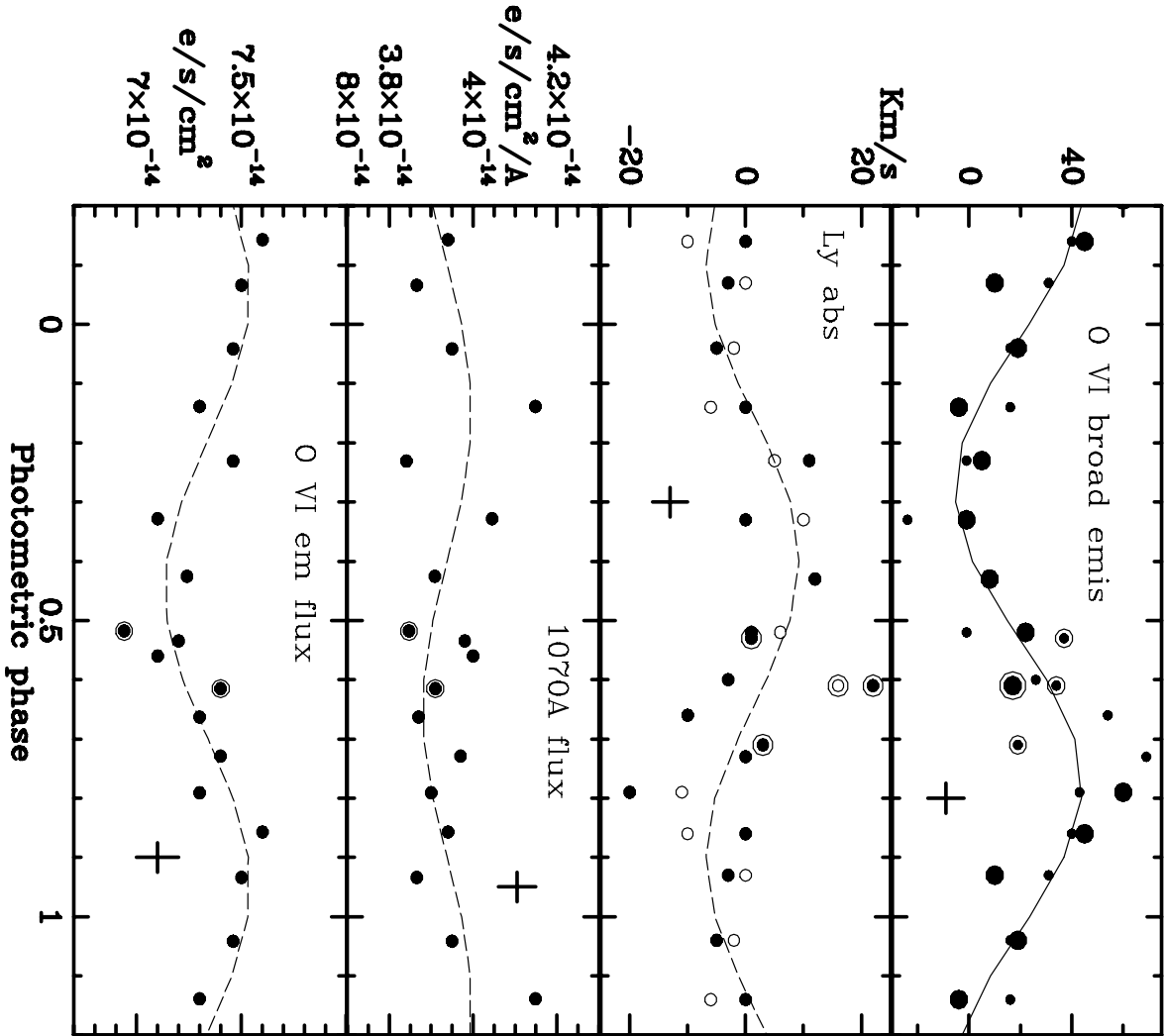


Fig. 4.— Individual velocity measures with superimposed best-fit sine curves. The circled points are those from the final overlapping phases in the observation sequence. In a few cases, measures were not possible or reliable due to data flaws, so not all quantities have 15 values plotted. The crosses show the average formal  $1\sigma$  errors and phase range for a measure. (top) O VI cross-correlation velocities from the LiF1A (large dots)

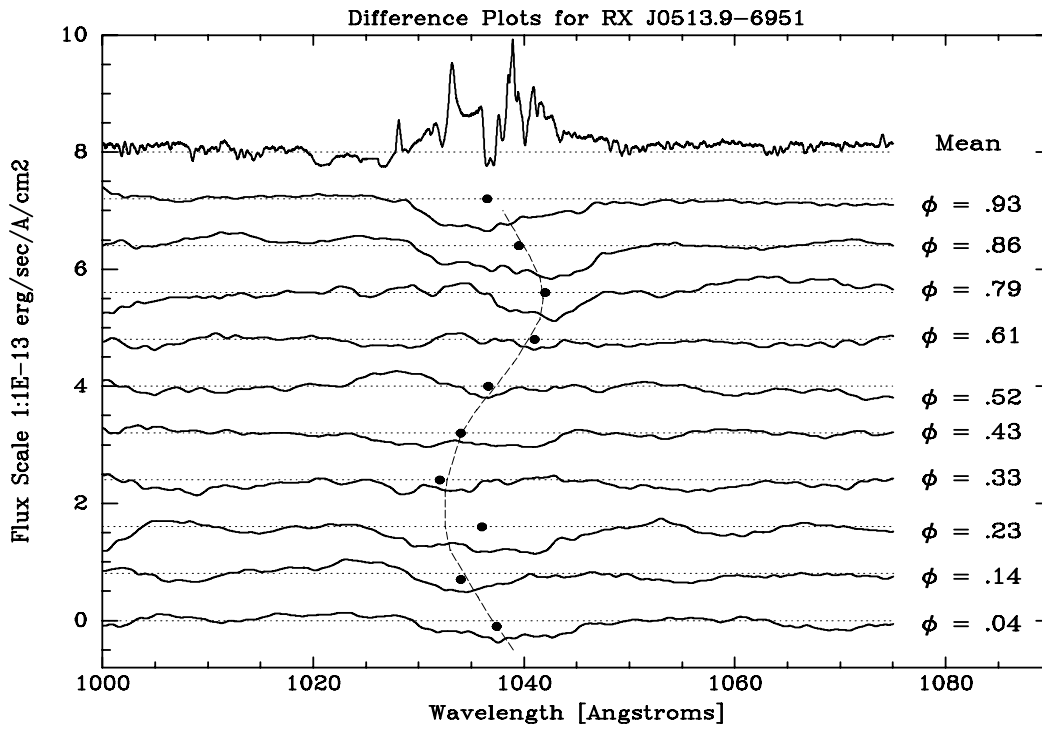


Fig. 5.— Mean spectrum (top) and differences from the mean obtained by subtracting the individual spectra. The difference spectra are smoothed over  $\sim 5\text{\AA}$  and expanded by a factor 5. The dots show the approximate centroids of the broad absorption feature, and the dashed curve illustrates a best-fit sine curve through them.

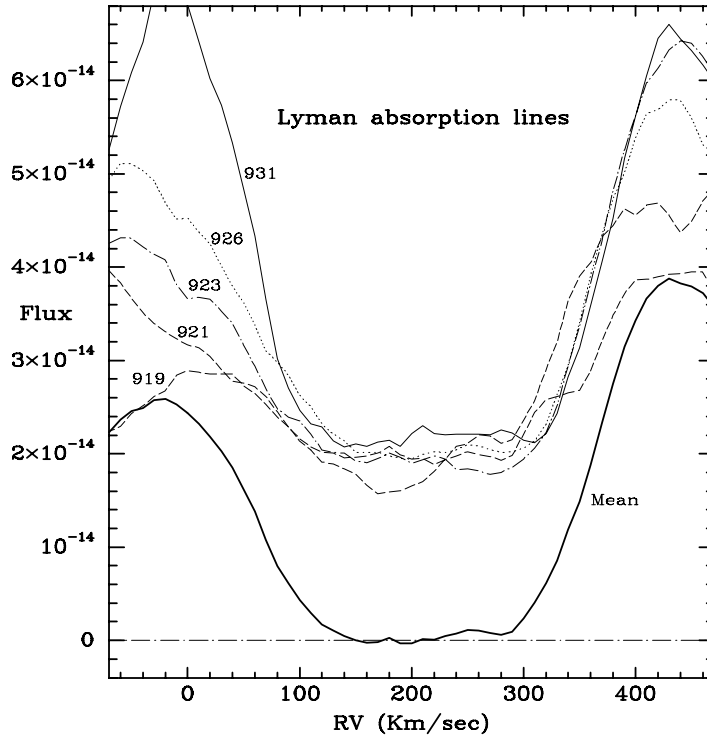


Fig. 6.— Profiles of the Lyman absorption lines least contaminated by airglow emission and H<sub>2</sub> absorption. Fluxes are in  $\text{erg cm}^{-2} \text{s}^{-1} \text{\AA}^{-1}$ . Each line is identified by its rest wavelength and shifted vertically by  $2 \cdot 10^{-14}$  to provide separation from the mean profile (shown as the heavy line). Note the flat-bottomed saturated absorption profiles and the large width in velocity.

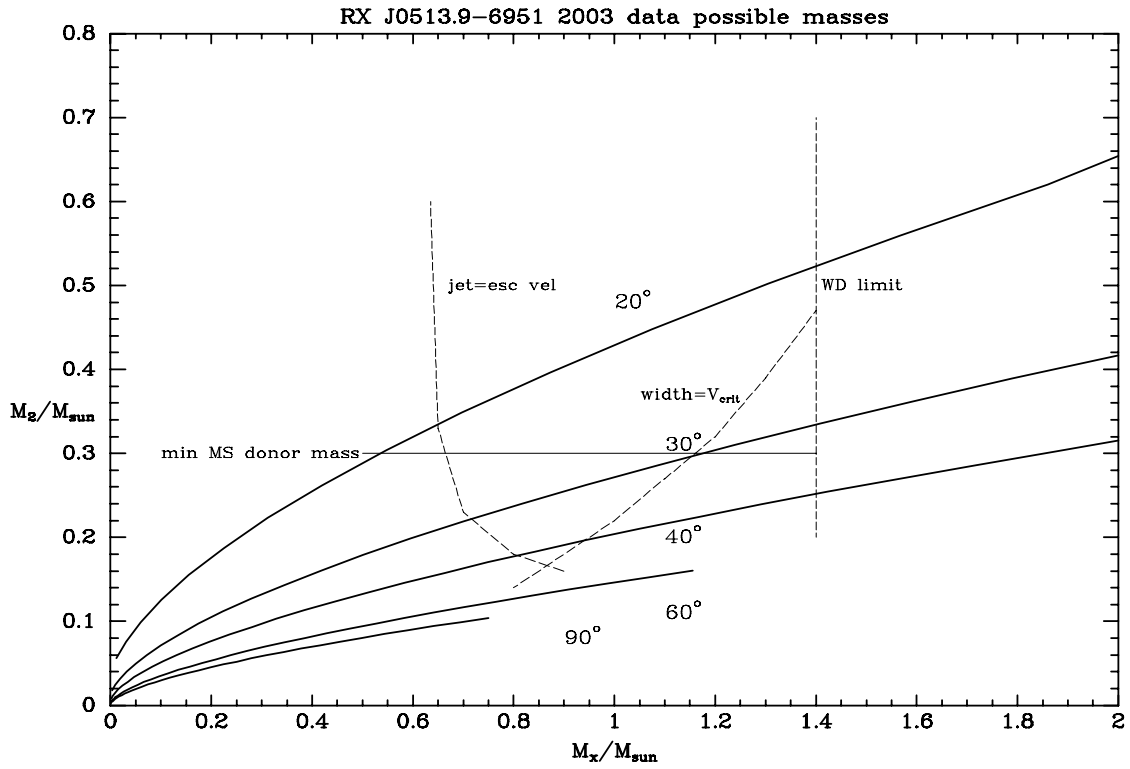


Fig. 7.— Mass diagram resulting from adopting the overall 2003 broad O VI emission velocity curve and assuming it traces the orbital motion of the compact star. The sketched limits arise from other considerations of the system, as described in the text.